IN SITU OBSERVATION OF EVAPORATING ICE CRYSTALS BY LASER TWO-BEAM INTERFEROMETRY

Takehiko Gonda[1] and Yuki Matsuura[2]

[1]*Division of General Education, Aichi Gakuin University, Iwasaki, Nisshin 470-01*
[2]*Toshiba Corporation, Research & Development Center, Komukai, Toshiba-cho, Saiwai-ku, Kawasaki 210*

Abstract: The evaporation rate of a polyhedral ice crystal is several times larger than the growth rate. The reason is because the slope of an evaporation pit P_e of the ice crystal is larger than the slope of a growth hillock P_g in addition to the increase of active sites of evaporation. The former means that the step separation of the evaporation pit λ_e is smaller than that of the growth hillock λ_g.

1. Introduction

Many natural snow crystals evaporate when snow crystals fall from the cloud base to the ground. Then, the tip shape of snow crystals observed is generally rounded (NAKAYA, 1954; KIKUCHI and UYEDA, 1987; HALLETT and KNIGHT, 1994). When ice crystals grow at considerably high supersaturation above water saturation, the tip shape of ice crystals, is also rounded (GONDA *et al.*, 1996). However, snow crystals with round tip will be scarcely formed in natural cloud because high supersaturation over water saturation does not occur in natural cloud. That is, snow crystals with faceted tip must grow in natural cloud. As described above, snow crystals will be exposed in air at or below ice saturation when snow crystals fall from the cloud base to the ground. Accordingly, it is important for meteorology to study the evaporation mechanism of snow crystals.

On the other hand, it has been experimentally found that the evaporation rate of an ice crystal was several times larger than the growth rate even under the same magnitude of driving force (GONDA and SEI, 1987), but the evaporation mechanism of the ice crystal has been unknown until now. In general, the growth rate of an ice crystal depends not only on supersaturation but also on the surface structure of the ice crystal (GONDA *et al.*, 1985), while the evaporation rate of an ice crystal depends on the evaporation conditions, and BECKMANN and LACMANN (1982) found that the evaporation rate of ice crystals was linear with subsaturation. In this study, we will discuss the evaporation mechanism by observing *in situ* evaporating ice crystal surfaces using a differential interference microscope and laser two-beam interferometry.

2. Experimental Method

A diagram of the experimental apparatus and the detail of a growth chamber were described in a previous paper (GONDA *et al.*, 1994, 1996). Accordingly, in this paper, only

the experimental method is described. The growth chamber was cooled by circulating isopropyl alcohol. In order to control precisely the temperature of an ice plate as the water vapor supplier and the growth substrate, an electric current which flows to the thermoelectric modules was automatically controlled (Gonda et al., 1996). The substrate temperature and the temperature difference between the ice plate and the substrate were measured using copper-constantan thermocouples. The measured values were automatically recorded in a microcomputer.

After the growth chamber was cooled to the specified temperature, a small amount of sufficiently diluted silver iodide smoke was inserted into the chamber. An ice crystal was grown in air at low pressure in order to grow the ice crystal under condition which can ignore the volume diffusion process of water molecules and the Berg effect. The growing and evaporating ice crystals were observed in situ using a differential interference microscope and laser two beam interferometry. The differential interference images and the interference fringes of equal thickness on the ice crystal surface were recorded by a video tape recorder.

3. Experimental Results

Figure 1 shows the (0001) face of an ice crystal evaporating just below ice saturation after growth up to the size of about 500μm in air of 5.3×10 P$_a$ at $-15°$C. Figure 1a is a differential interference image of the evaporating ice crystal. Figures 1b and c are the interference fringes of equal thickness. As seen in Fig. 1a, the ice crystal evaporates by the advance of evaporation steps from each edge to the center of the crystal. The ridges running from each corner and the middle of the edges to the center of the crystal were formed by the collision of evaporation steps. Some evaporation hillocks on the ridges were formed by the decrease of evaporation due to the adsorption of impurity vapor. When we observe the ice crystal surface using laser two-beam interferometry, it is seen that the interference fringes of equal thickness bend at the ridges and circular interference fringes are formed at evaporation hillocks. The circular interference fringes move from the outside of the evaporation hillocks to the inside.

Fig. 1. (0001) face of an ice crystal evaporating in air of 5.3×10 P$_a$ at $-15°$C and just below ice saturation. (a) Differential interference image. (b, c) Interference fringes of equal thickness. (a) 0, (b) 45, (c)79 s.

On the other hand, it is known that interference fringes of equal thickness formed by the evaporation pit move from the centers of the evaporation pits to the outside. Therefore, we can distinguish between the interference fringes forming on an evaporation hillock and those on the evaporation pit.

Figure 2 shows the ($10\bar{1}0$) face of an ice crystal evaporating at 1.0% subsaturation after growth up to the size of about 600 μm in air of 5.0 $\times$ 10 P_a and at $-15°C$. Figures 2a and c are the interference fringes of equal thickness formed on the evaporating ice crystal. Figure 2b is a differential interference image of the ice crystal. As seen in Fig. 2b, there are two evaporation pits at the middle and an evaporation pit at the upper right-hand side where dislocations emerge on the ($10\bar{1}0$) face. A curved line is the ridge formed by the collision of evaporation steps which advance from the center of each evaporation pit to the outside. As seen in Figs. 2a and c, when we observed the ($10\bar{1}0$) face using laser two-beam interferometry, as indicated by arrows, interference fringes of equal thickness bent at the center of each evaporation pit.

Figure 3 shows the ($10\bar{1}0$) face of an ice crystal evaporating with increasing subsaturation at the rate of 0.146%/s after growth up to about 600 μm in air of 5.0 $\times$ 10 P_a at

Fig. 2. ($10\bar{1}0$) face of an ice crystal evaporating in air of 5.0 $\times$ 10 P_a at $-15°C$ and 1.0% subsaturation. (a, c) Interference fringes of equal thickness. (b) Differential interference image. (a) 0, (b)16, (c) 60 s.

Fig. 3. ($10\bar{1}0$) face of an ice crystal evaporating in air of 5.0 $\times$ 10 P_a at $-15°C$ and with increasing subsaturation at the rate of 0.146%/s. (a) Differential interference image. (b, c) Interference fringes of equal thickness. (a) 0, (b) 23, (c) 40 s.

$-15°C$. Figure 3a shows a differential interference image of the $(10\bar{1}0)$ face. Figures 3b and c show interference fringes of equal thickness. Some evaporation pits formed at the positions where dislocations emerge on the $(10\bar{1}0)$ face are seen in Fig. 3a. In the figure, an arrow shows the direction along the c-axis. In Figs. 3b and c, circular interference fringes of equal thickness are formed when the slope of evaporation pits increases with increasing subsaturation. We can obtain the slope of evaporation pits by analyzing interference fringes of equal thickness (Gonda et al., 1966). Thus, the slope of the evaporation pit indicated by an arrow in Fig. 3b is $P_e = 2.65 \times 10^{-2}$ and that in Fig. 3c is $P_e = 3.02 \times 10^{-2}$.

4. Discussion

The evaporation rate of a polyhedral ice crystal is several times larger than the growth rate even under the same magnitude of driving force. In order to explain microscopically the experimental result, we observed *in situ* ice crystal surface evaporating after growth up to the size of 500–600 μm using a differential interference microscope and laser two-beam interferometry.

The chemical potential μ_c at the position where a dislocation outcrops on the crystal surface is larger than that at the ideal crystal surface. So, an evaporation pit is formed at the position where the dislocation emerges. As described in a former section, the slope of the evaporation pit P_e is of the order of 10^{-2}. This is one figure larger than the slope of the growth hillock $P_g \sim 10^{-3}$, which was formed at the same temperature (Gonda et al., 1994). The reason why the evaporation rate of a polyhedral ice crystal is several times larger than the growth rate can be explained mainly by the difference between the slope of the evaporation pit P_e and that of the growth hillock P_g.

Figure 4 shows a schematic diagram of an evaporation pit formed on evaporating ice crystal and a growth hillock formed on growing ice crystal. As shown in Fig. 4, the slope of the evaporation pit $P_e = \tan\theta_e$ is larger than that of growth hillock $P_g = \tan\theta_g$. Here, as the chemical potential of the ice crystal μ_c increases by the strain energy around a dislocation line, the driving force of evaporation $\Delta\mu_e = \mu_c - \mu_v$ becomes larger than that of growth $\Delta\mu_g = \mu_v - \mu_c$ within a small range around the dislocation, where μ_v is the chemical potential of the vapor phase. The rate of evaporation steps V_e is nearly equal to the rate of growth steps V_g (Chernov et al., 1986; Onuma et al., 1990). Accordingly, when the
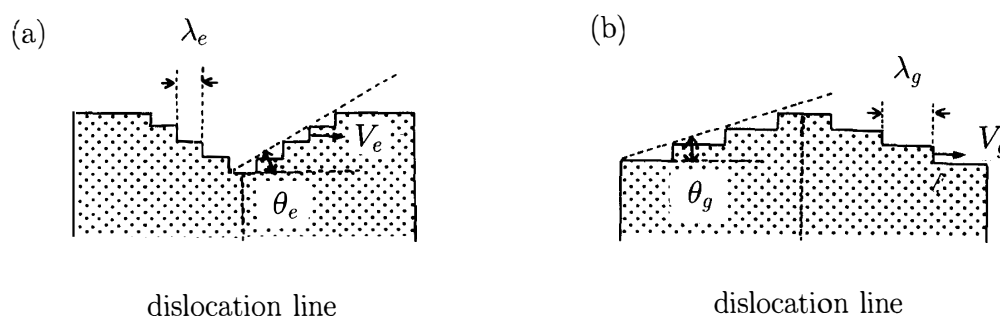

Fig. 4. *Schematic diagram of an evaporation pit and a growth hillock formed on ice crystal surface. (a) Evaporation pit. (b) Growth hillock.*

height of evaporation steps is equal to that of growth steps, $P_e > P_g$ corresponds to $\lambda_e < \lambda_g$, where λ_e is the step separation of the evaporation pit and λ_g is that of the growth hillock.

5. Conclusion

The evaporation rate of a polyhedral ice crystal is several times larger than the growth rate even under the same magnitude of driving force. The reason is because the slope of an evaporation pit P_e is larger than the slope of a growth hillock P_g in addition to the increase of active sites of evaporation. The former means that the step separation of the evaporation pit λ_e is smaller than that of the growth hillock λ_g.

References

BECKMANN, W. and LACMANN, R. (1982): Interface kinetics of the growth and evaporation of ice single crystals from the vapour phase. II Measurements in a pure water environment. J. Crystal Growth, 58, 433–442.

CHERNOV, A.A., RASCHKOVICH, I.N. and MKRTCHAN, A.A. (1986): Solution growth kinetics and mechanism: Prismatic face of ADP. J. Crystal Growth, 74, 101–112.

GONDA, T. and SEI, T. (1987): Evaporation form of ice crystals in subsaturated air and their evaporation mechanism. Proc. NIPR Symp. Polar Meteorol. Glaciol., 1, 113–121.

GONDA, T., SEI, T. and GOMI, H. (1985): Surface micromorphology of columnar ice crystals growing in air at high and low supersaturation. Mem. Natl Inst. Polar Res., Spec. Issue, 39, 108–116.

GONDA, T., MATSUURA, Y. and SEI, T. (1994): In situ observation of vapor-grown ice crystals by a laser two-beam interferometry. J. Crystal Growth, 142, 171–176.

GONDA, T., MATSUURA, Y. and WADA, M. (1996): Formation mechanism of plate-like ice crystals growing in air at low temperature and low supersaturation. Proc. NIPR Symp. Polar Meteorol. Glaciol., 10, 66–72.

HALLETT, J. and KNIGHT, C. (1994): On the symmetry of snow crystals. Atmos. Res., 32, 1–11.

KIKUCHI, K. and UYEDA, H. (1987): Formation mechanisms of eighteen-branched snow crystas. J. Fac. Sci. Hokkaido Univ., Ser. VII (Geophysics), 8(2), 109–119.

NAKAYA, U. (1954): Snow Crystals, Natural and Artificial. Cambridge, Harvard Univ. Press, 248–252.

ONUMA, K., TSUKAMOTO, K. and SUNAGAWA, I. (1990): Growth kinetics of K-alum crystals in relation to the surface supersaturations. J. Crystal Growth, 100, 125–132.